

Article

Microwave Absorption Properties of Ceramics Based on BiFeO₃ Modified with Ho

Pavel Astafev¹, Konstantin Andryushin^{1,2,*} , Aleksey Pavelko¹ , Alexander Lerer³ , Yakov Reizenkind¹, Ekaterina Glazunova¹, Lidiya Shilkina¹, Inna Andryushina¹, Alexandr Nagaenko⁴ and Larisa Reznichenko¹

¹ Research Institute of Physics, Southern Federal University, Stachki Ave., 194, 344090 Rostov-on-Don, Russia; astafev@sfnedu.ru (P.A.); aapavelko@sfnedu.ru (A.P.); jar@sfnedu.ru (Y.R.); glazunova@sfnedu.ru (E.G.); lid-shilkina@yandex.ru (L.S.); inandryushina@sfnedu.ru (I.A.); lareznichenko@sfnedu.ru (L.R.)

² Kh. Ibragimov Complex Institute of the Russian Academy of Sciences (CI RAS), Staropromyslovskoe hw., 21a, 364051 Grozny, Russia

³ Physical Faculty, Southern Federal University, Zorge Str., 5, 344090 Rostov-on-Don, Russia; lerer@sfnedu.ru

⁴ Institute of High Technology and Piezo Technic, Southern Federal University, Milchakova Str., 10, 344090 Rostov-on-Don, Russia; nagaenko@sfnedu.ru

* Correspondence: kpandryushin@gmail.com

Abstract: Ceramic samples of Bi_{1-x}Ho_xFeO₃, where $x = 0.00\text{--}0.50$, with a modifier concentration variation step $\Delta x = 0.05\text{--}0.10$, were prepared by a two-step solid-phase synthesis followed by sintering using conventional ceramic technology. X-ray phase analysis showed that all the solid solutions studied were formed in the presence of impurities. With increasing Ho concentration, a non-monotonic shift in all loss maxima towards the low-frequency region is observed, as well as an increase in their half-width. An increase in the external temperature leads to a monotonic shift in the absorption maxima towards the low-frequency region, which enables the necessary control of the microwave parameters in the X band. A conclusion has been drawn on the feasibility of using the data obtained in the design of new functional materials based on BiFeO₃, as well as devices with thermally controlled frequency.



Citation: Astafev, P.; Andryushin, K.; Pavelko, A.; Lerer, A.; Reizenkind, Y.; Glazunova, E.; Shilkina, L.; Andryushina, I.; Nagaenko, A.; Reznichenko, L. Microwave

Absorption Properties of Ceramics Based on BiFeO₃ Modified with Ho. *Solids* **2024**, *5*, 66–83. <https://doi.org/10.3390/solids5010005>

Academic Editor: Juan B. Carda Castelló

Received: 21 November 2023

Revised: 5 January 2024

Accepted: 12 January 2024

Published: 17 January 2024



Copyright: © 2024 by the authors. Licensee MDPI, Basel, Switzerland. This article is an open access article distributed under the terms and conditions of the Creative Commons Attribution (CC BY) license (<https://creativecommons.org/licenses/by/4.0/>).

Keywords: multiferroics; BiFeO₃; ceramic; microwave absorption; tuning

1. Introduction

In recent years, there has been a rapidly growing interest in a broad class of materials—BiFeO₃ (BFO)-based multiferroics—due to their combination of both antiferromagnetic (Neel temperature $T_N \sim 643$ K) and ferroelectric (Curie temperature $T_C \sim 1083$ K) properties [1–3]. The above can ensure their applicability as various microwave components or radio-absorbing coatings. However, the widespread introduction of this material is hampered by the difficulty of synthesizing thermally stable powder products suitable for obtaining the final object [4–6], as well as the presence of a spin-modulated structure which causes a weakening of the magnetization. The introduction of rare earth elements (REE) enables the structure of BiFeO₃ to be stabilized and its properties to be optimized [7].

Recently, Zhi-Ling Hou et al. [8] synthesized Ho-doped BiFeO₃ nanoparticles by the sol-gel method and showed by X-ray diffraction that the A sites are replaced by doping ions. This led to an increase in ferromagnetic properties, indicating cycloid disruption, as well as an increase in losses in the frequency range 2–18 GHz due to ferromagnetic resonance at microwave frequencies. Yong Li et al. [9] showed the effect of temperature on the thermal shift in the dielectric relaxation frequency in La/Nd-doped BFO nanoparticles in the X band from 300 to 673 K. It was also found that a change in temperature leads to a band shift in the microwave absorption covering almost the entire X band. C. Tian et al. [10] synthesized polycrystalline samples of Bi_{1-x}Sm_xFeO₃ ($x = 0.00, 0.05, 0.10, 0.15$) by the sol-gel method and showed that at $x = 0.10$ the material has good microwave absorption

properties, and the minimum reflection loss value of $\text{Bi}_{0.90}\text{Sm}_{0.10}\text{FeO}_3$ powder is about -32.9 dB at a frequency of 11.7 GHz, and its effective absorption band (RL (reflection loss) < -10 dB) is 2.6 GHz at the optimum tuning level.

Therefore, it seems relevant to prepare BiFeO_3 modified with rare earth elements in a wide range of concentrations by solid-phase synthesis methods followed by sintering using conventional ceramic technology and to study its microwave absorption in the temperature range 300–520 K to establish the possibility of controlling its properties by thermal action. Since preliminary studies on BiFeO_3 modified with Dy, Ho, Tb [11] showed that SS BiFeO_3 with Ho have the best microwave absorption, the concentration range of the specified modifier was extended in this work.

2. Materials and Methods

The objects of this study were solid solutions (SS) of the composition $\text{Bi}_{1-x}\text{Ho}_x\text{FeO}_3$ $x = 0.00$ – 0.50 and $\Delta x = 0.05$ – 0.10 . The samples were obtained using conventional ceramic technology (CCT), which includes a two-stage synthesis with intermediate grinding followed by sintering without applying pressure [12]. The selection of optimal technological modes was carried out on a series of experimental samples with X-ray control of the phase composition.

Bi_2O_3 , Fe_2O_3 , Ho_2O_3 oxides of high purity (AR, LR grade with a base content $> 99.95\%$) were used as starting reagents. Optimal conditions for synthesis and sintering of BiFeO_3 : $T_{\text{synt.1}} = T_{\text{synt.2}} = 1030$ K and holding times $\tau_{\text{synt.1}} = \tau_{\text{synt.2}} = 10$ h, $T_{\text{sint.}} = 1140$ K, $\tau_{\text{sint.}} = 2$ h. Optimal regimes for obtaining SS of composition $\text{Bi}_{1-x}\text{Ho}_x\text{FeO}_3$ $x = 0.05$ – 0.50 : $T_{\text{synt.1}} = 1070$ K ($x = 0.05$ – 0.20); $T_{\text{synt.2}} = 1090$ K ($x = 0.05$), $T_{\text{synt.2}} = 1110$ K ($x = 0.10$), $T_{\text{synt.2}} = 1130$ K ($x = 0.15$), $T_{\text{synt.2}} = 1150$ K ($x = 0.20$); $\tau_{\text{synt.1}} = \tau_{\text{synt.2}} = 10$ h; $T_{\text{sint.}} = 1180$ K ($x = 0.05, 0.10$), $T_{\text{sint.}} = 1200$ K ($x = 0.15, 0.20$), $\tau_{\text{sint.}} = 1.5$ h (Table 1) [13]. Mechanical activation (MA) of synthesized SS powders with $x = 0.30$ – 0.50 was carried out at the stage of production of press powders prepared for sintering. MA was carried out in a high-energy grinding planetary ball mill AGO-2. The grinding was carried out in an alcoholic medium for 15 min, the drum rotation speed was 1820 rpm.

Table 1. Phase composition and optimal conditions of SS ceramics $(\text{Bi}_{1-x}\text{Ho}_x)\text{FeO}_3$ [13].

Composition	$T_{\text{synt.1}}$, K	$T_{\text{synt.2}}$, K	$T_{\text{sint.}}$, K	Phase Composition, $I_{\text{imp.}}/I_{\text{pr}}$
$x = 0.00$	1030	1030	1140	12 $\text{Bi}_{25}\text{FeO}_{40}$ + 11 $\text{Bi}_2\text{Fe}_4\text{O}_9$
$x = 0.05$	1070	1090	1180	12 $\text{Bi}_{25}\text{FeO}_{40}$ + 10 $\text{Bi}_2\text{Fe}_4\text{O}_9$
$x = 0.10$	1070	1110	1180	9 $\text{Bi}_{25}\text{FeO}_{40}$ + ~20 $\text{Ho}_3\text{Fe}_5\text{O}_{12}$
$x = 0.15$	1070	1130	1200	17 $\text{Bi}_{25}\text{FeO}_{40}$ + ~30 $\text{Ho}_3\text{Fe}_5\text{O}_{12}$
$x = 0.20$	1070	1150	1200	24 $\text{Bi}_{25}\text{FeO}_{40}$ + ~45 $\text{Ho}_3\text{Fe}_5\text{O}_{12}$

Tables 2 and 3 show the process of optimizing the conditions for obtaining the SS of the $\text{Bi}_{1-x}\text{Ho}_x\text{FeO}_3$ system with $x = 0.30$ – 0.50 . It can be seen that at $T_{\text{synt.1}} = 870$ K, in the solution with $x = 0.30$, $\text{Bi}_{25}\text{FeO}_{40}$ is formed as the main phase, and BiFeO_3 and Ho_2O_3 , which did not participate in the reaction, are also formed in small amounts. When the temperature is increased to $T_{\text{synt.1}} = 1120$ K, BiFeO_3 becomes the main phase and the composition of the impurity phase changes to $\text{Bi}_2\text{Fe}_4\text{O}_9$ and HoFeO_3 . In SS with $x = 0.40$ and $x = 0.50$ at first synthesis temperatures $T_{\text{synt.1}} = 1020$ – 1070 K, BiHoO_3 and HoFeO_3 act as the main phase. Bismuth ferrite is only formed as the main phase at temperatures of the second synthesis $T_{\text{synt.1}} = 1070$ – 1120 K.

Table 2. Optimization of synthesis conditions for $\text{Bi}_{1-x}\text{Ho}_x\text{FeO}_3$ (Without MA).

Composition	$T_{\text{synt.1}} = 870 \text{ K}$	$T_{\text{synt.1}} = 1020 \text{ K}$	$T_{\text{synt.1}} = 1070 \text{ K}$	$T_{\text{synt.2}} = 1070 \text{ K}$ ($T_{\text{synt.1}} = 870 \text{ K}$)	$T_{\text{synt.2}} = 1120 \text{ K}$ ($T_{\text{synt.1}} = 1070 \text{ K}$)
$x = 0.30$	100 $\text{Bi}_{25}\text{FeO}_{40}$ + 34 Ho_2O_3 + 38 BiFeO_3	100 BiFeO_3 + 85 $\text{Bi}_2\text{Fe}_4\text{O}_9$ + 72 HoFeO_3 +	100 BiFeO_3 + 60 HoFeO_3	100 BiFeO_3 + 14 $\text{Bi}_{25}\text{FeO}_{40}$ + 25 HoFeO_3	100 BiFeO_3 + 10 $\text{Bi}_{25}\text{FeO}_{40}$ + 38 HoFeO_3
$x = 0.40$	100 $\text{Bi}_{25}\text{FeO}_{40}$ + 71 Ho_2O_3 + 38 BiFeO_3	100 $\text{Bi}_2\text{Fe}_4\text{O}_9$ + 84 HoFeO_3 + 100 BiHoO_3	92 BiFeO_3 + 41 $\text{Bi}_2\text{Fe}_4\text{O}_9$ + 100 HoFeO_3	100 BiFeO_3 + 10 $\text{Bi}_{25}\text{FeO}_{40}$ + 30 HoFeO_3	100 BiFeO_3 + 15 $\text{Bi}_{25}\text{FeO}_{40}$ + 63 HoFeO_3
$x = 0.50$	100 $\text{Bi}_{25}\text{FeO}_{40}$ + 83 Ho_2O_3 + 33 BiFeO_3	100 $\text{Bi}_2\text{Fe}_4\text{O}_9$ + 84 HoFeO_3 + 100 BiHoO_3	26 BiFeO_3 + 91 $\text{Bi}_2\text{Fe}_4\text{O}_9$ + 100 HoFeO_3	100 BiFeO_3 + 16 $\text{Bi}_{25}\text{FeO}_{40}$ + 90 HoFeO_3	100 BiFeO_3 + 14 $\text{Bi}_{25}\text{FeO}_{40}$ + 70 HoFeO_3

Table 3. Optimization of synthesis conditions for $\text{Bi}_{1-x}\text{Ho}_x\text{FeO}_3$ (With MA).

Composition	$T_{\text{synt.1}} = 870 \text{ K}$	$T_{\text{synt.1}} = 1020 \text{ K}$	$T_{\text{synt.1}} = 1070 \text{ K}$	$T_{\text{synt.2}} = 1070 \text{ K}$ ($T_{\text{synt.1}} = 870 \text{ K}$)	$T_{\text{synt.2}} = 1070 \text{ K}$ ($T_{\text{synt.1}} = 1020 \text{ K}$)	$T_{\text{synt.2}} = 1120 \text{ K}$ ($T_{\text{synt.1}} = 1070 \text{ K}$)	$T_{\text{synt.2}} = 1170 \text{ K}$ ($T_{\text{synt.1}} = 1070 \text{ K}$)
$x = 0.30$	100 $\text{Bi}_{25}\text{FeO}_{40}$ + 36 Ho_2O_3 + 38 BiFeO_3	100 BiFeO_3 + 17 $\text{Bi}_{25}\text{FeO}_{40}$ + 27 HoFeO_3	100 BiFeO_3 + 25 $\text{Bi}_{25}\text{FeO}_{40}$	100 BiFeO_3 + 15 Bi_2O_3	100 BiFeO_3 + 27 ($\text{Bi}_{25}\text{FeO}_{40}$ + HoFeO_3)	100 BiFeO_3 + 19 $\text{Bi}_{25}\text{FeO}_{40}$ + 15 phase mixture	100 BiFeO_3 + 18 Bi_2O_3 + 26 $\text{Ho}_3\text{Fe}_5\text{O}_{12}$
$x = 0.40$		100 BiFeO_3 + 65 phase mixture			100 BiFeO_3 + 10 $\text{Bi}_{25}\text{FeO}_{40}$ + 94 HoFeO_3		
$x = 0.50$		15 BiFeO_3 + 100 $\text{Bi}_2\text{Fe}_4\text{O}_9$ + 60 phase mixture			100 BiFeO_3 + 15 $\text{Bi}_{25}\text{FeO}_{40}$ + 64 HoFeO_3		

In SS with $x = 0.30$, the use of mechanical activation favours the incorporation of Ho into the BiFeO_3 structure, which occurs gradually as the temperature of the first synthesis is increased to 1070 K. With a further increase in the synthesis temperature, the number of impurity phases increases again, indicating their decomposition. In SS with $x = 0.40$ and $x = 0.50$, mechanical activation did not give a positive result. The positive result of the use of mechanical activation appeared only in the case of SS with $x = 0.30$.

The sintered ceramic pieces were subjected to mechanical processing (cutting along a plane, grinding and polishing along flat surfaces and ends) in order to obtain cylindrical measurement samples with a diameter of 10 mm and a height of 1 mm. Each composition contained (8–10) such samples.

X-ray studies were carried out by powder diffraction on a DRON-3 diffractometer ($\text{CoK}\alpha$ radiation) with an installed IR-2 X-ray intensimeter, connected to a PC and equipped with special software developed by an employee of the organization for a specific device. Ground ceramic objects were studied, which made it possible to exclude the influence of surface effects, stresses and textures that occur during the production of ceramics. The structural parameters were calculated using standard methods [14]. The errors in the measurements of the structural parameters had the following values: linear $\Delta a = \Delta b = \Delta c = \pm (0.002\text{--}0.004) \text{ \AA}$; angular $\Delta\beta = 3'$; volume $\Delta V = \pm 0.05 \text{ \AA}^3$ ($\Delta V/V \cdot 100\% = 0.07\%$), C—cubic phase, Pcs—pseudocubic. Sample density was determined by the Archimedean method using *N*-octane.

To study the microstructure of the cleavages of the samples, a JSM-6390L scanning electron microscope (JEOL, Tokyo, Japan) with a system of microanalyzers (Oxford Instruments, Abingdon, Great Britain) was used. The resolution of the microscope is up to 1.2 nm at an accelerating voltage of 30 kV (image in secondary electrons), the limits of the accelerating voltage are from 0.5 kV to 30 kV, the magnification is from $\times 10$ to $\times 1,000,000$, the beam current is up to 200 nA. The grain landscape was also studied using a KEYENCE VK-9700 color laser scanning 3D microscope (KEYENCE, Osaka, Japan) and a Hitachi TM1000 electron microscope (Hitachi, Marunouchi, Japan).

Microwave studies were carried out using a P9375A “Keysight” vector network analyzer (VNA) (Keysight, Santa Rosa, CA, USA), which has an operating frequency range of 300 kHz–26.5 GHz, and a waveguide measuring cell. Instrument calibration was performed using the X11644A “Keysight” calibration kit (Keysight, Santa Rosa, CA, USA).

A waveguide measurement cell was used to measure the samples, consisting of a 23×10 mm (X band, (8.2–12.4) GHz) waveguide line with a heating element insulated by plates of heat-resistant material. The sample was placed in the center of the waveguide, in the H plane, using a rectangular insert made of fireclay bricks, completely filling the section of the waveguide (Figure 1).

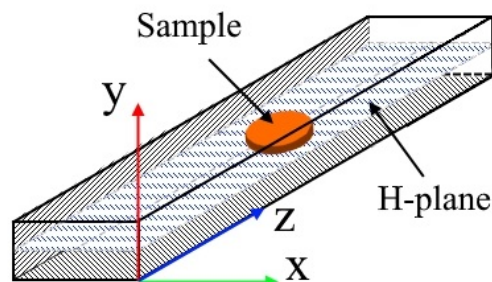


Figure 1. Scheme of the sample location in the waveguide.

Coaxial waveguide junctions (CWJs) from the calibration kit were used to connect the measurement cell to the VNA measurement cables.

Forward (d_F) and reverse (d_R) loss factors were calculated using the following formula [15–17]:

$$d_{F,R} = 1 - \left| S_{11(22)} \right|^2 - \left| S_{21(12)} \right|^2, \quad (1)$$

where $\left| S_{11(22)} \right|^2$ and $\left| S_{21(12)} \right|^2$ are the squared modules of the elements of the quadripole scattering matrix, expressed in relative units, which have the physical meaning of the power reflection coefficient and the power transmittance coefficient, respectively. These parameters were determined during the experiment.

Reflection coefficients (S_{11} , S_{22}) in an empty waveguide measuring cell over the entire frequency range do not exceed -20 dB (Figure 2a), and direct and return losses are no more than 10% (Figure 2b). The indicated level of agreement is satisfactory within the framework of this experiment. Reflection coefficient pulsations (S_{11} , S_{22}) with a small frequency step are probably associated with the interference of waves reflected from the junctions of the coaxial cables with the coaxial-to-waveguide transition (CWT) and the measurement cell with the CWT. In all the following figures, all the ripples associated with the technical characteristics are filtered by the moving average method. It should also be noted that the level of the forward and return losses is the same, which indicates the symmetry of the 4-port network measured.

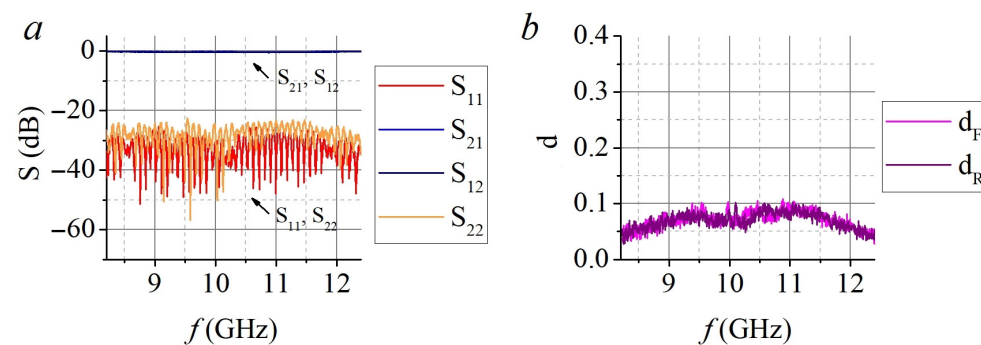


Figure 2. Dependences of S-parameters (a) and forward and return loss coefficient (b) of an empty waveguide measuring cell on frequency at room temperature.

The presence of a measuring insert (made of fireclay brick) in the waveguide leads to an increase in the reflection coefficients (S_{11} , S_{22}) up to -10 dB (Figure 3a), as well as an increase in direct (d_F) and reverse (d_R) losses by 10% (here and other percentages relative to the power of the incident electromagnetic wave) (approximately 2 times) (Figure 3b) in comparison with the parameters of an empty measuring cell (Figure 2). The minima of the reflection coefficient are caused by the interference of reflected waves from the air–material interface of the insert. The $d_{F,R}$ maxima at frequencies (11–12.4) GHz are probably due to the resonance of the electromagnetic wave in the sample hole.

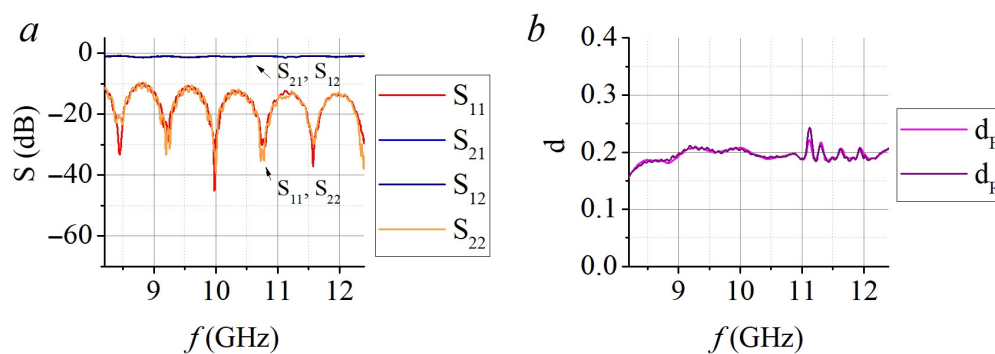


Figure 3. Dependences of the S-parameters (a) and the forward and return loss coefficients (b) of a waveguide test cell with insert on the frequency at room temperature.

At high temperatures, the level of losses in an empty waveguide measurement cell (curve wg 503 K in Figure 4) remains almost unchanged compared to similar studies at room temperature (curve wg 302 K in Figure 4). At the same time, the level of losses in the waveguide measurement cell with a measuring insert when exposed to temperature (curve i503 K in Figure 4) is 10% higher compared to similar measurements at room temperature (curve i302 K in Figure 4). The increase in loss is probably due to an increase in the imaginary part of the dielectric constant of the insert material with increasing temperature.

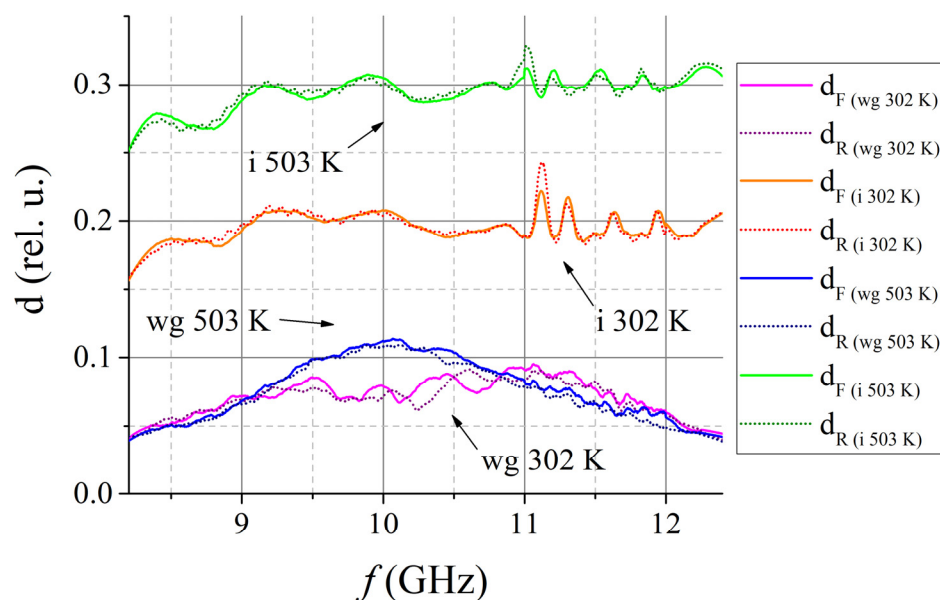


Figure 4. Frequency dependence of the forward and return loss coefficients of an empty waveguide (wg—waveguide) and an insert (i—insert) at room (302 K) and elevated (502 K) temperatures.

Considering the small changes in the loss level of an empty waveguide test cell with increasing temperature, it is possible to exclude its influence on the level of losses

introduced into the system by calculating the difference between the loss coefficients of the filled insert and the empty test cell:

$$D_i = d_{i(av)} - d_{wg(av)}, \quad (2)$$

where D_i is the electromagnetic loss coefficient in the measuring insert, $d_{i(av)}$ is the average loss value in the measuring cell with the insert, $d_{wg(av)}$ is the average loss value in the empty waveguide measuring cell. $d_{i(av)}$ and $d_{wg(av)}$ were calculated as the arithmetic mean of the forward and reverse loss coefficients, which is due to their similarity for all the experiments performed (in our case the system is a symmetrical four-port network). Previously, this method was used by a team of authors to evaluate the microwave absorption of ferroelectric ceramic materials [18]. The absorption parameters of materials can therefore be considered either as losses of the whole system or as differential losses due to the presence of an experimental sample in the measurement cell.

The dynamics of changes in the microwave response of the measuring insert with increasing temperature can be assessed by analyzing the dependence of D_i in the measuring insert as a function of frequency and temperature (Figure 5a). For ease of analysis, the data obtained are presented in the form of a heat map (Figure 5b), which is a top view of the image (Figure 5a) (loss maxima on the heat map are light areas, minima are dark).

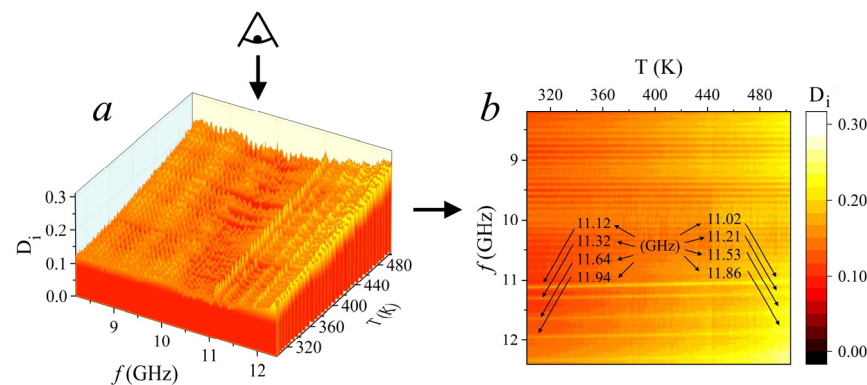


Figure 5. Dependences of D of fireclay insert on frequency, f , and temperature T . (b) is a heat map based on the data in (a) and is presented as a top view.

When the waveguide is heated with the probe, all maxima of D_i shift monotonically to the low-frequency region on ~ 100 MHz, so that the maxima at the frequencies 11.12 GHz and 11.94 GHz at high temperature are at the frequencies 11.02 GHz and 11.86 GHz. This is probably due to an increase in the value of the real part of the dielectric constant of the insert material with increasing temperature.

This section may be divided by subheadings. It should provide a concise and precise description of the experimental results, their interpretation, as well as the experimental conclusions that can be drawn.

3. Results and Discussion

$\text{Bi}_{1-x}\text{Ho}_x\text{FeO}_3$ samples with $x = 0.00$ – 0.20 and $\Delta x = 0.05$ contain two impurity phases $\text{Bi}_{25}\text{FeO}_{40}$ and $\text{Bi}_2\text{Fe}_4\text{O}_9$, and relative density (ρ_{rel}) is in the range 83.78–88.33 depending on x . The work [13] present the results of previous studies. Figure 6 show X-ray diffraction patterns of $\text{Bi}_{1-x}\text{Ho}_x\text{FeO}_3$ SS with $x = 0.30$ – 0.50 . It can be seen that, a SS with a perovskite-type structure without impurity phases has not been formed; moreover, the perovskite structure itself has not been fully formed in all SS. The content of impurities increases with increasing x . The relative intensities of the $\text{Bi}_{36}\text{Fe}_2\text{O}_{57}$ peaks are 34, 41, 50 in samples with $x = 0.30, 0.40, 0.50$, respectively. The ρ_{rel} of the ceramics with $x = 0.30, 0.40, 0.50$ are 89, 82, 86%, respectively.

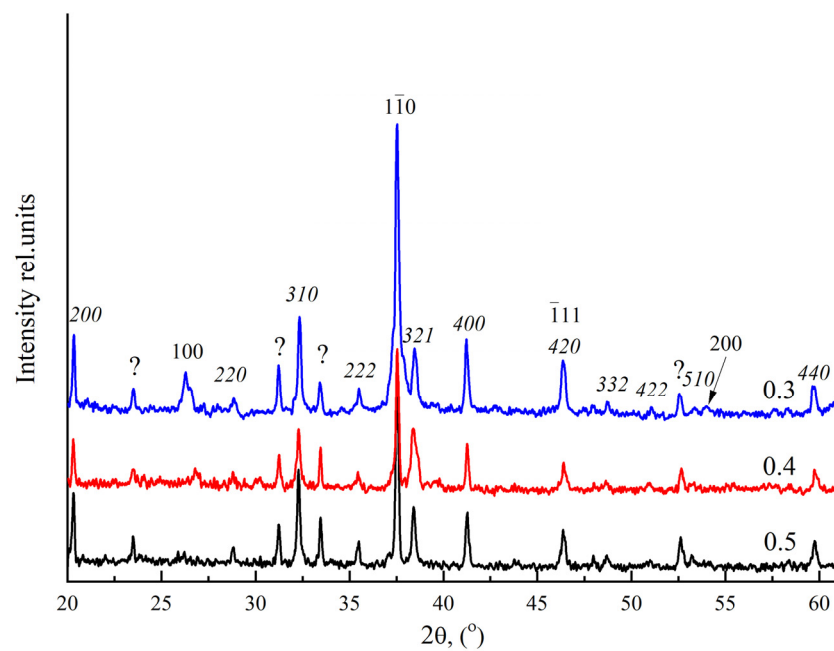


Figure 6. X-ray diffraction patterns of $\text{Bi}_{1-x}\text{Ho}_x\text{FeO}_3$ SS, x values are shown on the X-ray diffraction patterns. Straight indices indicate diffraction reflections of the SS with perovskite structure. Indices of diffraction reflections of the compound $\text{Bi}_{36}\text{Fe}_2\text{O}_{57}$ (PDF set 42, card 181) are shown in italics; the sign “?” marks diffraction peaks that could not be identified.

The result obtained is not unexpected, since the substitution $\text{Bi}^{3+} \leftrightarrow \text{Ho}^{3+}$ does not satisfy the empirical rules of Goldschmidt isomorphism: the difference in ionic radii, ΔR , is not more than 15%, the difference in electronegativity, ΔEN , is not more than 0.4.

In this SS, ΔR is 39% ($\text{Bi}^{3+} = 1.20$, $R \text{Ho}^{3+} = 0.86$ for c. n. 6 according to Belov-Bokiy [19]) and $\Delta EN = 0.8$, in such cases only microisomorphism is possible [20]. The cell parameter of the perovskite phase, calculated from a single diffraction reflection of 110, is the same for all SS: $a = 3.948 \text{ \AA}$, and is smaller than the BiFeO_3 parameter, $a = 3.959 \text{ \AA}$ (PDF set 14, card 181), by $\Delta = 0.011 \text{ \AA}$. This suggests that a small amount of Ho nevertheless replaces Bi in the SS structure, since the ionic radius of Ho^{3+} is smaller than that of Bi^{3+} . The remainder of the Ho is probably part of an unidentified impurity phase.

Figures 7–9 show fragments of the microstructure of ceramic samples of bismuth ferrite containing holmium (Ho) in the composition $\text{Bi}_{1-x}\text{Ho}_x\text{FeO}_3$ $x = 0.30$ (Figure 7), $x = 0.40$ (Figure 8), $x = 0.50$ (Figure 9) (previously in [13] the grain structure in ceramics was studied with $0.00 \leq x \leq 0.20$). In each of the figures, different views of the same object are shown at different scales.

In all cases, the heterogeneity of the grain landscape is noted with crystallites whose habit is parallelepiped (“tiles”) or cube (larger grains are highlighted with dashed lines in Figure 7a–c) or formations of indeterminate shape (near cubic, small grains). In each case, the size of the large and small grains is noted several times (sometimes by an order of magnitude). The size of large grains increases as the bismuth ferrite is enriched with holmium from $\sim 4 \mu\text{m}$ ($x = 0.30$) to $\sim 10 \mu\text{m}$ ($x = 0.50$), and the size of small grains decreases slightly, remaining in the range (0.5–1.0) μm . The packing of the grains is chaotic, loose in places (Figure 8c,f), areas of looseness (highlighted by dashed lines) with areas of denser structures (Figure 8g, dashed lines), sometimes in the form of radial ring areas (Figure 7c), winding lines).

An increase in the concentration of introduced holmium leads, in addition to the enlargement of plate-like grains, to the conglomeration of small grains (Figure 8b,d, dashed lines) at $x = 0.40$ and subsequently ($x = 0.50$) to an increase in their number and the displacement of large crystallites (Figure 9b–e).

The fact that during the recrystallization sintering process, in all the cases considered, grains of almost regular geometric shape are formed, with clear edges, indicates that they grow in the bulk, in which, in addition to solid grains and gaseous pores, there is a liquid phase (LP), in which the grains are immersed [21]. In most cases, such ideomorphic grains are characteristic of secondary discontinuous recrystallization processes, in which impurities located at the grain boundary at the recrystallization temperature form a liquid phase that actively interacts with the base material, acting not so much as a “lubricant” as a transport medium, i.e., a solvent. The selective growth of large grains in this case is due to ordinary dissolution and precipitation from solution, not to boundary movement. In this case, the liquid covering the surface of such grains with a film causes them to acquire a certain growth form and regular cut, identical to the habit of crystals growing from a molten solution. As a result, idiomorphic grains crystallize in the form of polyhedra with almost straight edges [22].

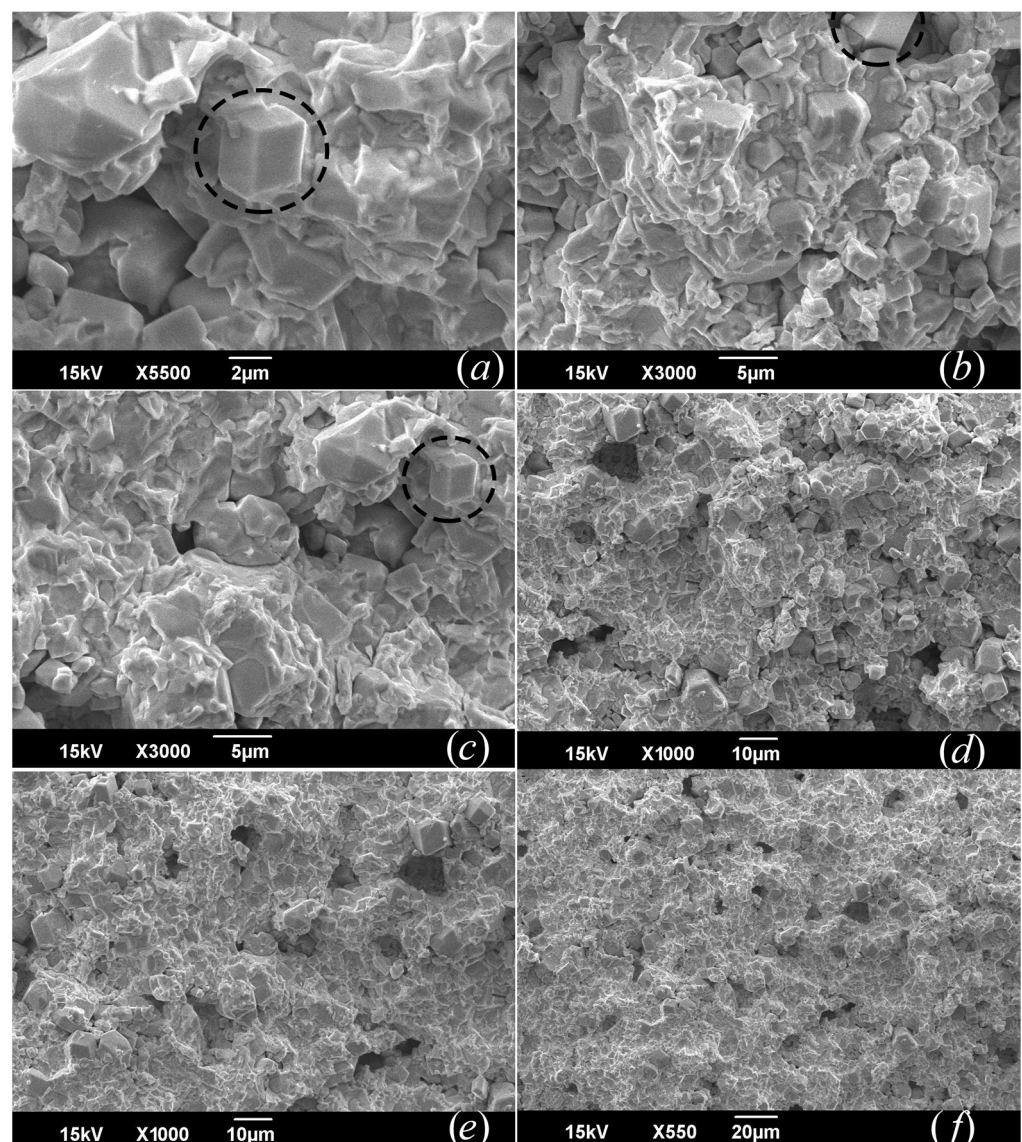


Figure 7. Fragments of the microstructure of the ceramic SS $\text{Bi}_{0.70}\text{Ho}_{0.30}\text{FeO}_3$. (a–f) are different views of the same object shown at different scales. Areas of interest are indicated by a dashed line and are described in the text.

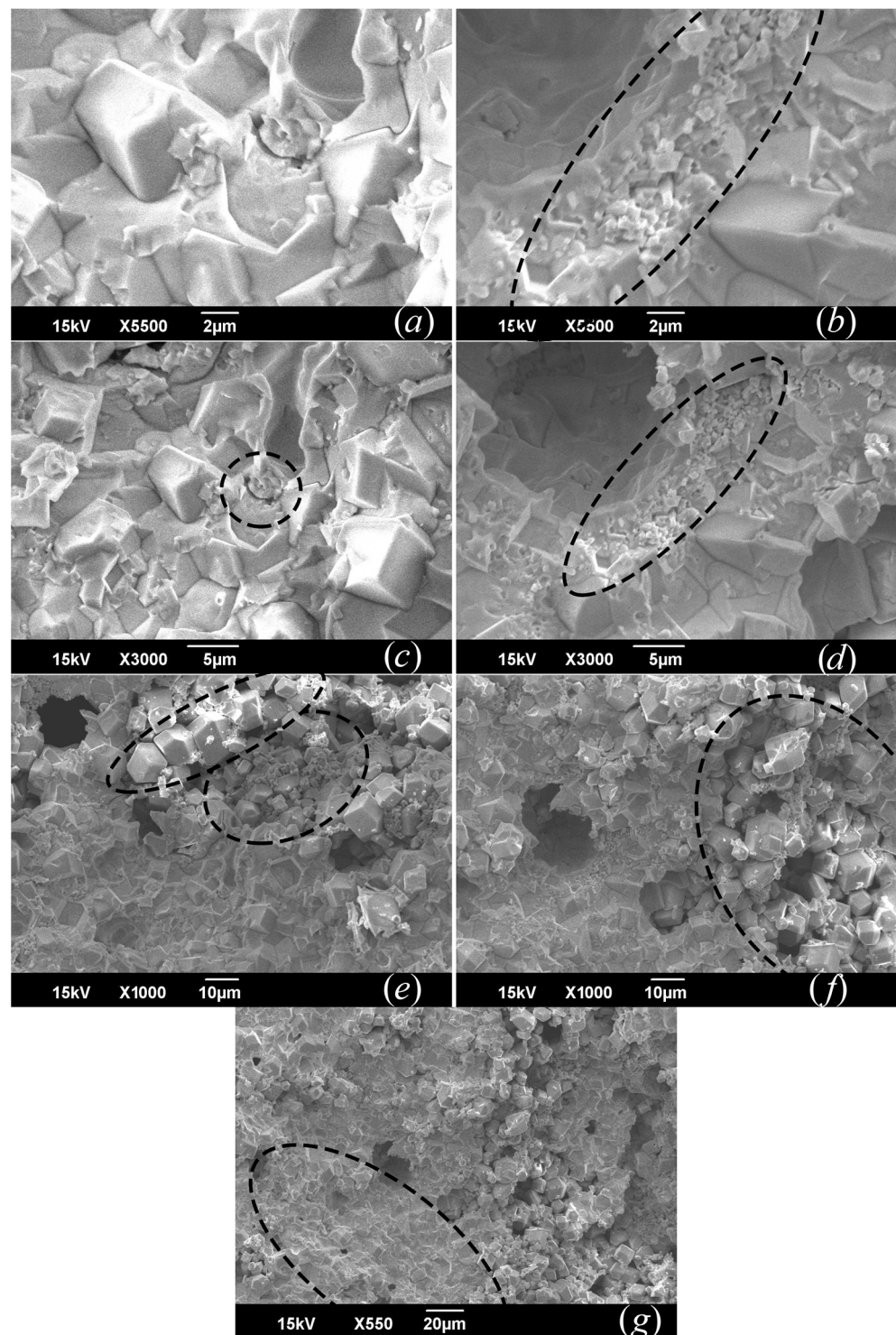


Figure 8. Fragments of the microstructure of the ceramic SS $\text{Bi}_{0.60}\text{Ho}_{0.40}\text{FeO}_3$. (a–g) are different views of the same object shown at different scales. Areas of interest are indicated by a dashed line and are described in the text.

The formation of the liquid phase may be related to the presence of unreacted bismuth oxide, Bi_2O_3 , with a low melting point, $T_{\text{melt.}} = 1098 \text{ K}$, in the mixtures of the studied materials, as well as to the composition of $\text{Fe}_2\text{O}_3\text{-Bi}_2\text{O}_3$, T_{melt} which may be even lower than in Bi_2O_3 (see figure from [23]).

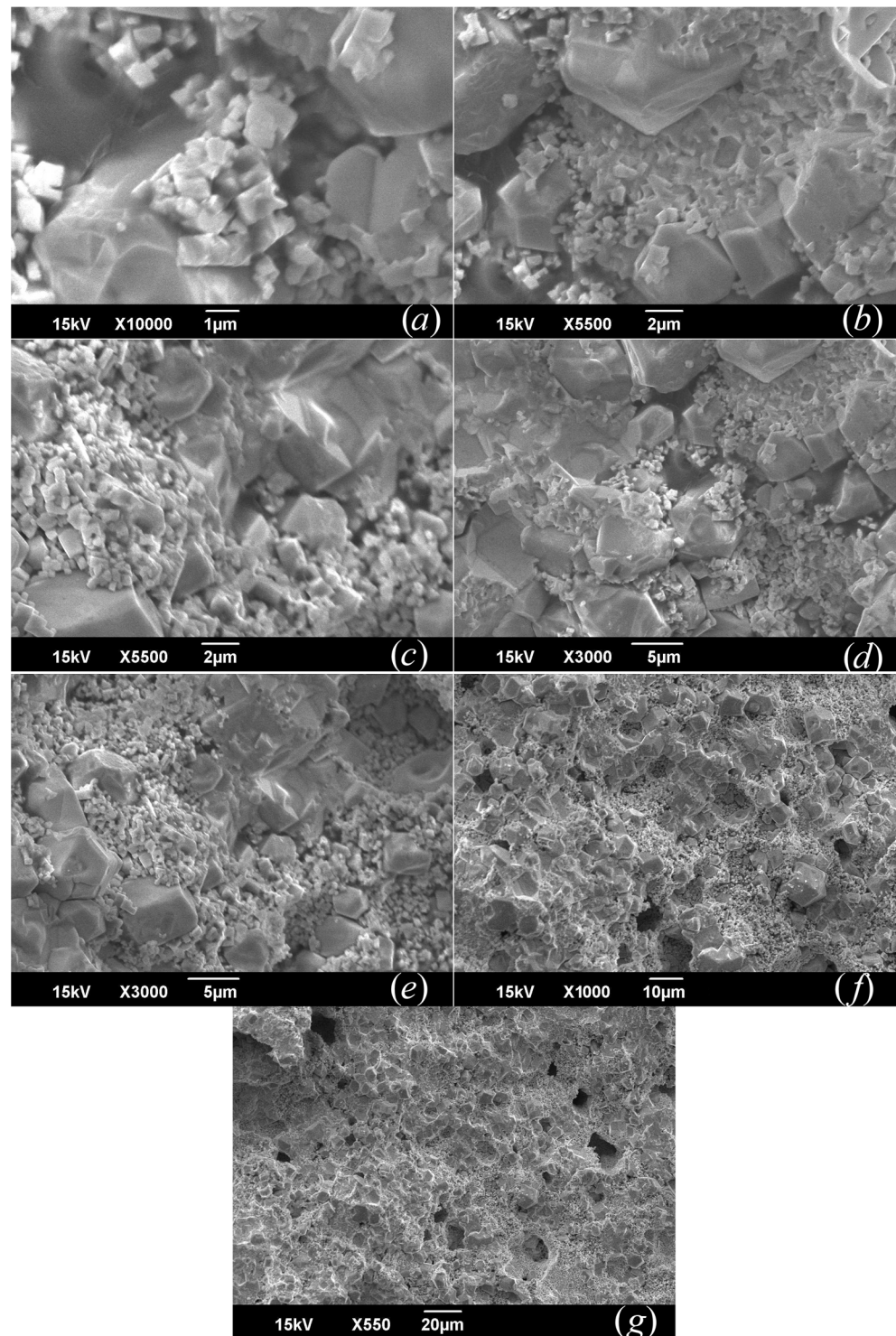


Figure 9. Fragments of the microstructure of the ceramic SS $\text{Bi}_{0.50}\text{Ho}_{0.50}\text{FeO}_3$. (a–g) are different views of the same object shown at different scales.

The results of this study are as follows the microwave absorption properties of ceramic samples of BiFeO_3 with different amounts of Ho, where in all cases the electromagnetic loss coefficient D has been calculated according to Formula (2), where instead of $d_{i(av)}$ —the average value of the losses in the measurement cell with an empty insert—a similar coefficient obtained for a measurement cell with a sample of the material under study has been used. When studying the microwave absorption of ceramic samples of original and

modified BiFeO₃, it was found that, in addition to the features previously observed when measuring an empty insert (maxima marked with number 1 in Figure 10), the measuring insert with sample has additional loss maxima due to the presence of samples in the measuring insert (maxima marked with number 2 in Figure 10).

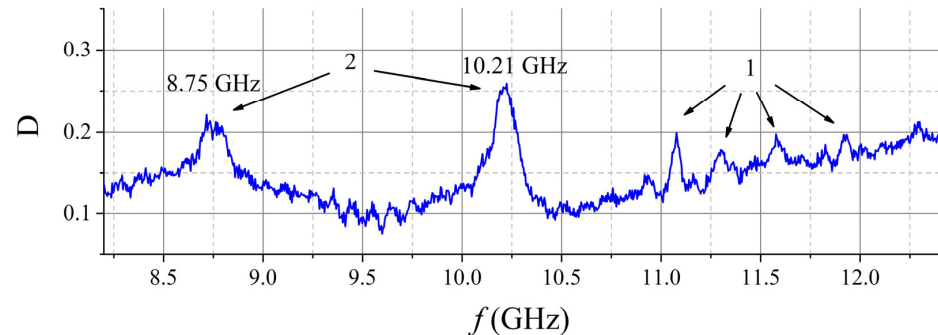


Figure 10. Frequency dependence of the loss coefficient (D) of the insert with a BiFeO₃ sample (1—maxima due to the presence of the insert; 2—maxima due to the presence of the sample).

In particular, for the original BiFeO₃, these maxima are located at frequencies of 8.75 GHz and 10.21 GHz and it is difficult to determine their nature unambiguously from the data obtained. They can be of both resonant and non-resonant nature. However, by studying the dynamics of changes in the position and intensity of these maxima, it is possible to draw some tentative conclusions about the process of changing the values of the complex dielectric and magnetic permeability in their vicinity. The reason for the shift in the position of the maxima in the frequency domain is a change in the length of the electromagnetic wave, λ , in the material: $\lambda = 1/\sqrt{\epsilon'\mu'}$, where ϵ' and μ' are the real parts of the dielectric and magnetic permeabilities, respectively. A decrease in intensity and an increase in the half-width of the maxima, as well as an increase in the general background losses, indicate an increase in the imaginary part of the dielectric (ϵ'') and magnetic (μ'') permeabilities. We then analyzed the dynamics of changes in the microwave response of samples of the materials under investigation as a function of Ho concentration and temperature.

First, the dependence of the loss coefficient (D) of the insert with a BiFeO₃ sample on frequency (f) and temperature (T) was analyzed. In order to assess the dynamics of the changes in the microwave response of the material with increasing temperature, plots similar to Figure 5b. To assess the temperature hysteresis of the microwave response dependence on temperature, the dependence was plotted for both the heating mode (Figure 11a) and the cooling mode (Figure 11b). With increasing temperature, the maxima D of the sample (maxima 1 and 2—M1 and M2—in Figure 11 and below) shift linearly towards the lower-frequency region, while their intensity increases.

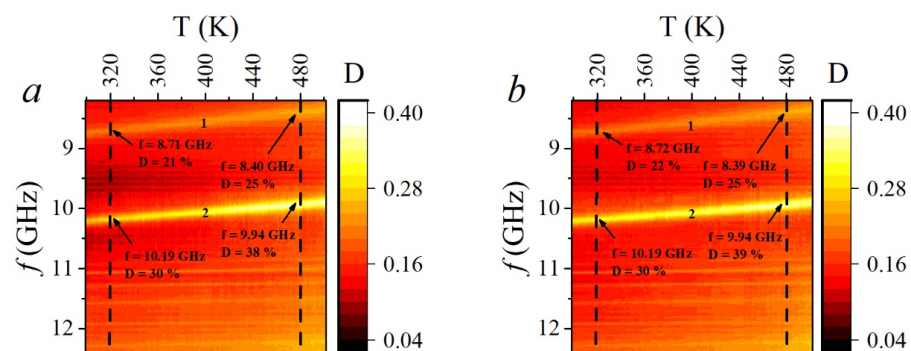


Figure 11. Dependence of the loss coefficient (D) of the insert with a BiFeO₃ sample on frequency (f) and temperature (T) ((a)—heating; (b)—cooling; numbers 1 and 2 indicate the maxima due to the presence of the sample in the insert).

Both during heating and cooling, the dynamics of the changes in intensity and frequency of the loss maxima are the same, so there is no temperature hysteresis in the material under study. However, in order to avoid unnecessary inaccuracies due to inadequate temperature control, 320 K and 480 K have been chosen here and below as the reference temperatures for the comparative analysis. The shift in the frequency domain when the sample is heated from 320 K to 480 K is 320 MHz for the first maximum and 250 MHz for the second. The increase in intensity is 4% for the first maximum and 8% for the second. The shift in the position of the loss maxima in the frequency domain is probably due to an increase in the value of the real part of the dielectric or magnetic permeability of the insert material with increasing temperature. The increase in the height of the maxima is probably related to an increase in the value of the imaginary part of the dielectric or magnetic permeability of the sample material with increasing temperature [9]. It is not possible to unambiguously determine the contribution of magnetic and dielectric permittivity to the position and intensity of the loss maxima from the data obtained. The difference between the positions of the peaks is 1.47 GHz at low and 1.55 GHz at high temperatures.

With the introduction of 5 mol% Ho, the D maxima have a significantly larger half-width but lower intensity (Figure 12), probably due to an increase in ϵ'' and μ'' . When the sample is heated from 320 K to 480 K, the shift in M1 is 280 MHz, for M2—250 MHz, and the increase in intensity is ~5% and ~9%, respectively. It was found that in the temperature range of ~320 K the distance between the maxima in the frequency domain is 1.42 GHz and 1.46 GHz at ~480 K. It is shown that in the dependence of D on temperature during cooling, an intensity hysteresis is observed in the vicinity of the M2 frequencies (Figure 12b), and its intensity and half-width do not return to their original form (Figure 12a). This is probably due to the memory effects of the material.

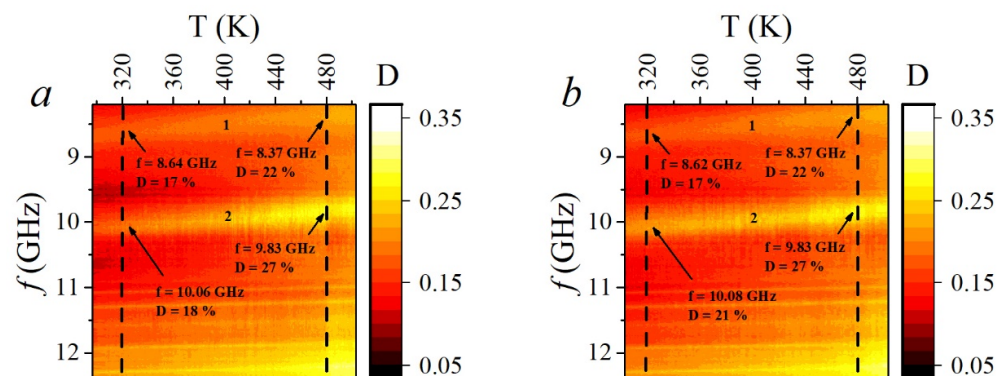


Figure 12. Dependence of the loss coefficient (D) of the measuring insert with a BiFeO_3 sample modified with 5 mol. % Ho, on frequency (f) and temperature (T) ((a)—heating; (b)—cooling; numbers 1 and 2 indicate maximums due to the presence of a sample in the measuring insert).

When $x = 0.10$ is introduced (Figure 13), the M2 intensity in the samples is on average 5% higher. When the sample was heated from 320 K to 480 K, the shift was ~270 MHz and ~260 MHz for M1 and M2, respectively. At the same time, the increase in intensity was about 3% and 7%, respectively. The distance between the maxima, compared to $x = 0.05$, did not change practically and was 1.44 GHz at low temperatures and 1.45 GHz at high temperatures. It should be noted that the behavior of the sample with $x = 0.10$ is similar to the case of BiFeO_3 with 5 mol% of Ho, as upon cooling an intensity hysteresis is observed in the vicinity of the frequencies of the first and second maxima (Figure 13b).

At $x = 0.15$, the high-frequency maximum (Figure 14, marked with number 2) is significantly shifted to the low-frequency region compared to the data obtained for objects with $x < 0.15$ (Figures 11–13), while the distance between M1 and M2 is much smaller, being 0.95 GHz at ~320 K and 1 GHz at ~480 K.

In addition, the intensity of M2 increased significantly while the values for M1 remained at the same level. The bias when heating the sample from 320 K to 480 K is

190 MHz for M1 and 250 MHz for M2. In this case the intensity increased by 2% for M1 and 3% for M2 compared to $x = 0.10$ (Figure 13). It was found that compared to $x < 0.15$ (Figures 11–13), both the shift in the D maxima and the increase in their intensity with increasing temperature decreased significantly.

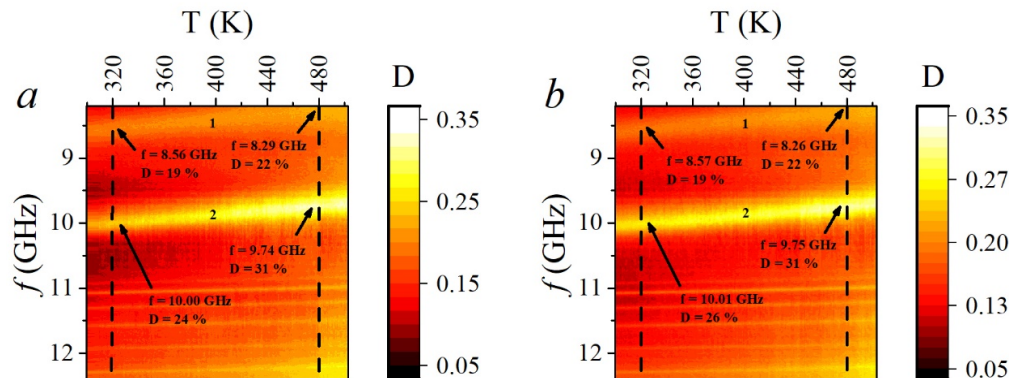


Figure 13. Dependences of the loss coefficient (D) of the measuring insert with a BiFeO₃ sample modified with 10 mol. % Ho, on frequency (f) and temperature (T) ((a)—heating; (b)—cooling; numbers 1 and 2 indicate maxima due to the presence of a sample in the measuring insert).

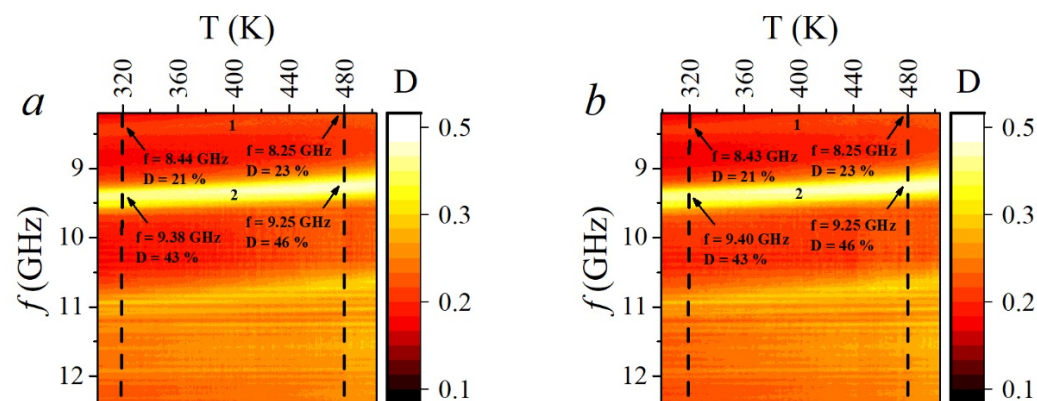


Figure 14. Dependences of the loss coefficient (D) of the measuring insert with a BiFeO₃ sample modified with 15 mol. % Ho, on frequency (f) and temperature (T) ((a)—heating; (b)—cooling; numbers 1 and 2 indicate maxima due to the presence of a sample in the measuring insert).

At $x = 0.20$, the low-frequency maximum (M1) is absent (Figure 15), probably due to either its significant shift to the low-frequency region, beyond the measurement range, or a decrease in its intensity to the general loss level. It was found that the shift in the maximum when the sample is heated from 320 K to 480 K is 200 MHz and the increase in intensity is 3%. Therefore, as in the case of SS with $x = 0.15$ (Figure 14), a small frequency shift in the D maximum and a change in its intensity were observed.

At $x = 0.30$, the intensity of the second maximum (Figure 16) is comparable to the value obtained for SS with $x = 0.15$ (Figure 14), and averages 50%, and its shift when heating the sample from 320 K to 480 K is less than at $x = 0.15$ – 0.20 (Figures 14 and 15) and is carried out within 120 MHz. The increase in its intensity is $\sim 3\%$.

It should be noted that in samples with $x = 0.30$, two additional high-frequency maxima are observed (maxima marked with numbers 3 and 4 in Figure 17), which are of low intensity. At lower holmium concentrations, these features were not found.

At $x = 0.40$ (Figure 18), maxima 3 and 4 have higher intensity in contrast to samples with $x = 0.30$. The shift in maximum 2 when the sample is heated from 320 K to 480 K is less than 50 MHz and the increase in intensity is $\sim 4\%$. The shift in the third and fourth maxima is also small, 20 and 30 MHz, respectively.

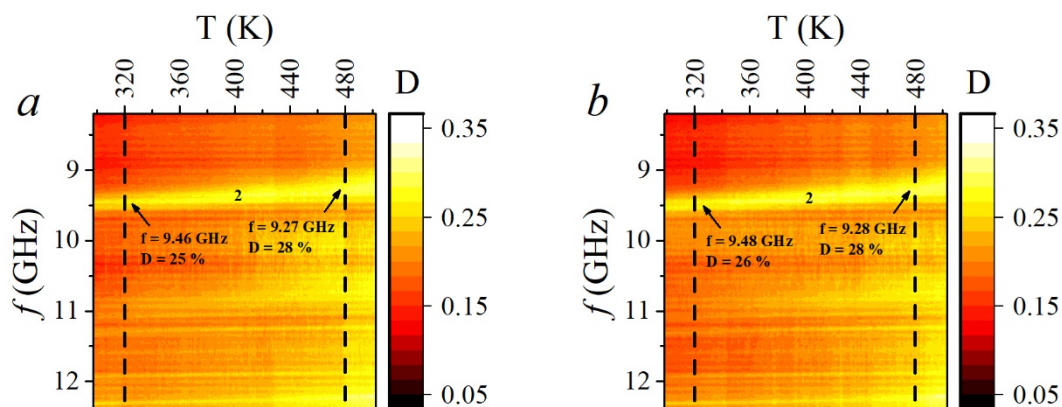


Figure 15. Dependences of the loss coefficient (D) of the measuring insert with a BiFeO_3 sample modified with 20 mol. % Ho, on frequency (f) and temperature (T) ((a)—heating; (b)—cooling; numbers 1 and 2 indicate maximums due to the presence of a sample in the measuring insert).

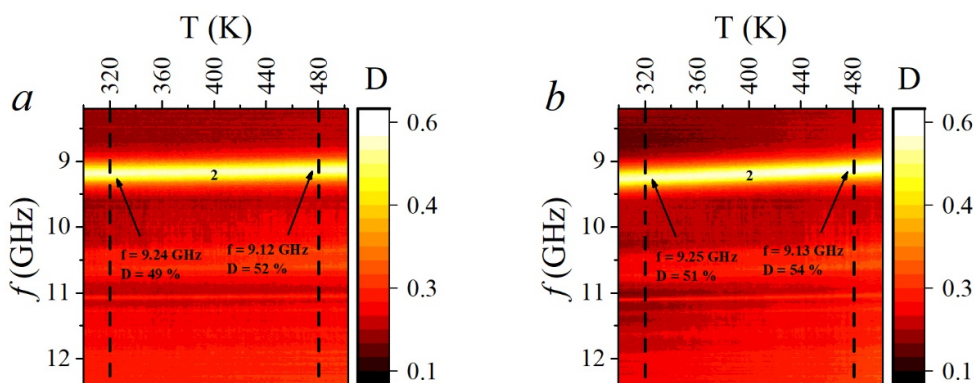


Figure 16. Dependences of the loss coefficient (D) of the measuring insert with a BiFeO_3 sample modified with 30 mol. % Ho, on frequency (f) and temperature (T) ((a)—heating; (b)—cooling; numbers 1 and 2 indicate maximums due to the presence of a sample in the measuring insert).

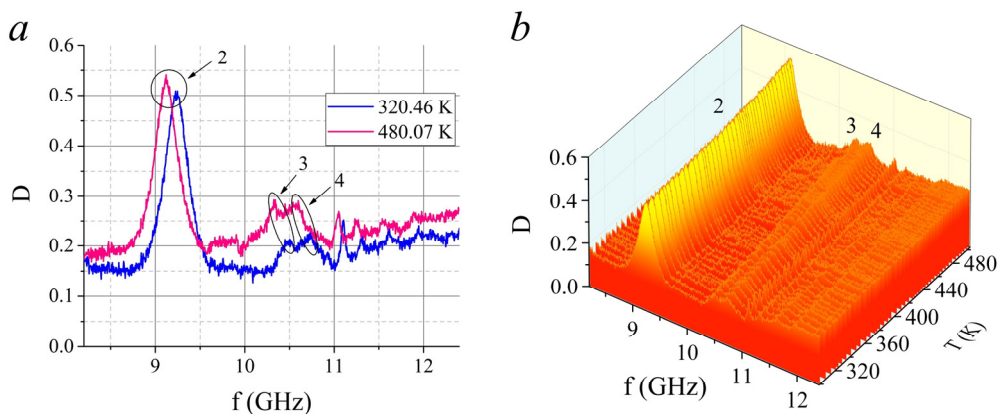


Figure 17. Dependences of the loss coefficient (D) of the measuring insert with a BiFeO_3 sample modified with 30% Ho on frequency (f) (a) and on f and temperature (T) (b) (numbers 2, 3 and 4 indicate maxima due to the presence of the sample in the measuring insert). The color gradient in figure b serves to indicate high and low values of D , but does not indicate specific values that are located on the left vertical axis.

It should be noted that the dynamics of the changes in the microwave response of the ceramic SS with $x = 0.50$ (Figure 19) with increasing temperature is similar to that of the BiFeO_3 modified with 40 mol% Ho (Figure 18). The shift in the second maximum in the

frequency domain when the sample is heated from 320 K to 480 K is small and amounts to less than 50 MHz.

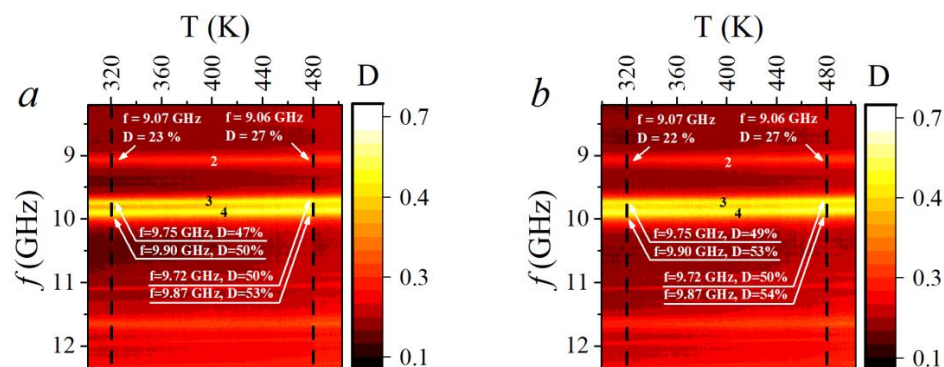


Figure 18. Dependence of the loss coefficient (D) of the measuring insert with a BiFeO_3 sample modified with 40 mol. % Ho, on frequency (f) and temperature (T) ((a)—heating; (b)—cooling; numbers 2, 3 and 4 indicate the maxima due to the presence of the sample in the measuring insert).

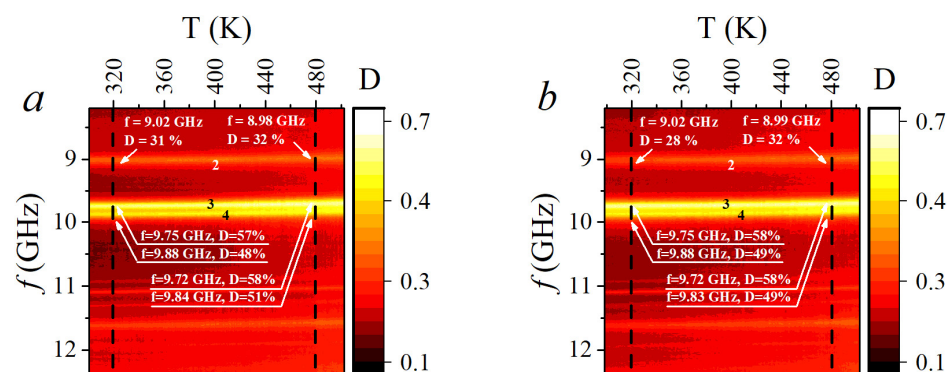


Figure 19. Dependence of the loss coefficient (D) of the measuring insert with a BiFeO_3 sample modified with 50 mol. % Ho, on frequency (f) and temperature (T) ((a)—heating; (b)—cooling; numbers 2, 3 and 4 indicate the maxima due to the presence of the sample in the measuring insert).

Since the main observed variables were the frequencies and intensities of loss maxima, as well as their shift and increase in intensity with increasing temperature, to summarize the results obtained, these parameters are presented depending on the concentration of the modifier (Figure 20). It is clear (Figure 20a) that the shift in the loss maxima with increasing modifier concentration is non-monotonic, indicating a non-monotonic increase in ϵ' with increasing modifier concentration. However, it should be noted that when the modifier concentration reaches $\sim 30\%$ or more, the shift in the maxima in the frequency domain practically stops, which is probably due to the dispersion of λ .

The method used in our work to determine reflection losses associated with interferences is not without drawbacks, as in [8], but it does enable us to clarify the nature of the absorption maxima that occur. In the present study, no losses were detected in the vicinity of $\sim 8\text{--}9$ GHz, but the detected anomalies at other frequencies are likely to be due to interferences at the sample boundary or resonance. Further research using other methods and sample shapes is required to clarify this hypothesis.

When a small amount of Ho $x \leq 0.05$ is added, the half-width of the loss maxima in the sample increases sharply while their intensity decreases (Figure 20b). A further increase in the concentration of Ho $x = 0.05\text{--}0.20$ leads to an increase in the intensity of the loss maxima, as well as an increase in the total background, while maintaining the half-width of the peaks. This is probably due to an increase in ϵ'' and μ'' in the microwave region as the concentration of the modifier changes. At $x = 0.20$ and above, the loss maxima observed at small x shift out of the frequency measurement window and all other loss maxima behave stochastically.

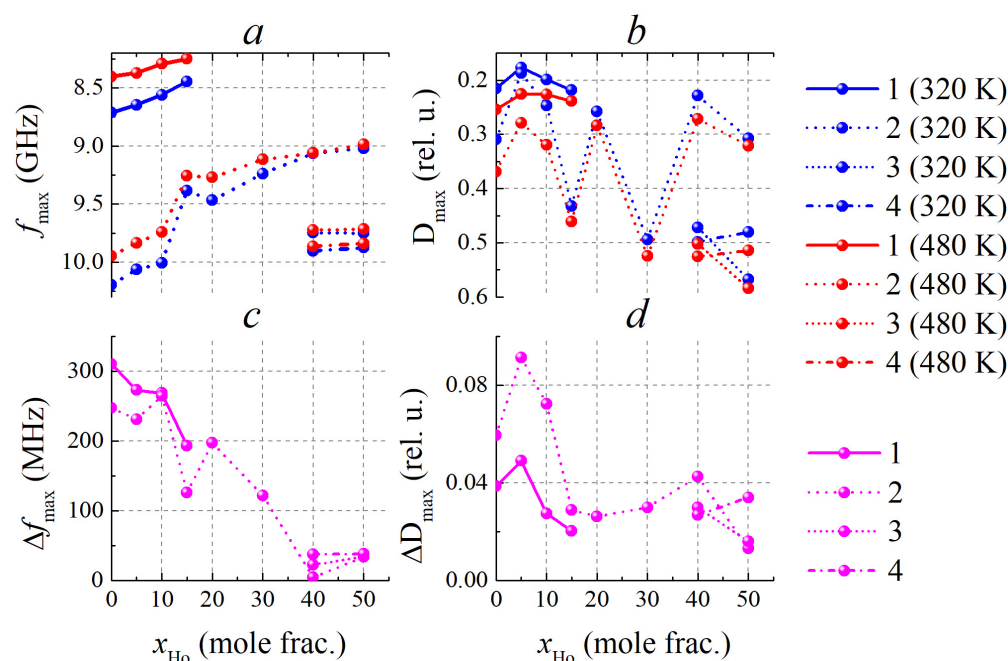


Figure 20. Dependence of the frequency (a) and intensity (b) of the maxima of electromagnetic losses (D) of modified BiFeO_3 at $T = 320$ K and $T = 480$ K, as well as the shift in the frequency of the maximum (c) and the increase in its intensity (d) when heated from 320 K to 480 K from Ho concentration.

Using X-ray data from [13] for $\text{Bi}_{1-x}\text{Ho}_x\text{FeO}_3$ with $x = 0.00$ – 0.20 , as well as data obtained in this work for $x = 0.30$ – 0.50 , it is possible to detect a correlation between the relative density of the solid solution and the intensity of the loss maxima, especially the second one (Figure 21).

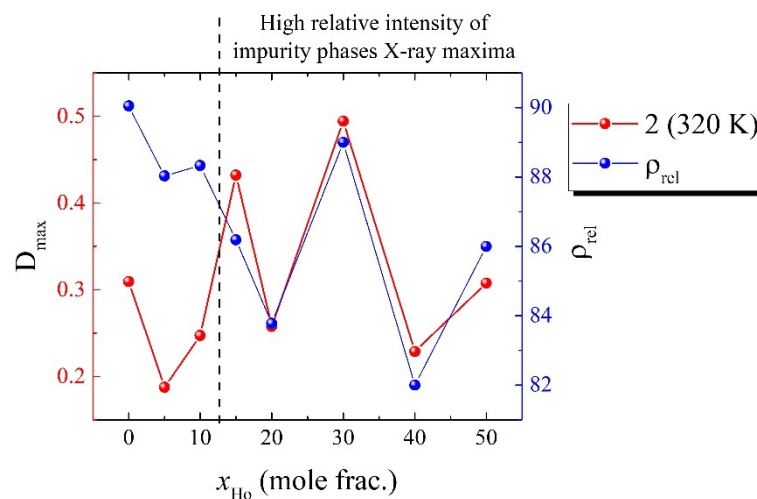


Figure 21. Dependence of the height of the second loss maximum (D_{max}) at 320 K (line marked “2 (320 K)”) and the relative density (ρ_{rel}) on the Ho concentration (x). The dotted line indicates the approximate limit beyond which the impurity phases begin to have a significant effect on the losses in the material.

In compositions with a higher relative density, as well as with a higher relative intensity of the X-ray maxima of the impurity phases, a higher level of loss maxima is observed, indicating a significant influence of the homogeneity (rather stoichiometry) of the elemental composition on the losses in the materials studied. In the case of SS with $x = 0.00$ – 0.10 , the correlation shown is like that of SS with $x = 0.15$ – 0.50 , but the level of maximum losses is lower in the first case. This indicates the existence of a certain boundary between the base

perovskite and the impurity phases, near which an increase in the amount of impurities leads to a sharp increase in the level of losses.

It should be noted that the microstructural features at high Ho content ($x = 0.30\text{--}0.50$) have no visible effect on the absorption properties of the objects studied.

4. Conclusions

Ceramic samples of $\text{Bi}_{1-x}\text{Ho}_x\text{FeO}_3$, where $x = 0.00\text{--}0.50$, $\Delta x = 0.05\text{--}0.10$, were prepared by a two-step solid-phase synthesis followed by sintering using conventional ceramic technology. It was found that all the SS studied were formed in the presence of impurities. Analyzing all the data obtained, several conclusions can be drawn.

- (1) As the Ho concentration increases to ~ 20 mol%, there is a non-monotonic shift in all loss maxima towards the low-frequency region, probably due to an increase in the real part of the dielectric or magnetic permeability of the studied material in the microwave range, and as $\sim 30\%$ or more is reached, the shift in the maxima in the frequency range practically stops, probably due to the dispersion λ .
- (2) Materials with high levels of impurities are characterized by high losses.
- (3) A monotonic increase in the intensity of the loss maxima and a monotonic shift in their position towards the low-frequency region with increasing temperature is observed in all samples studied. This indicates a monotonic increase in the complex dielectric or magnetic permeability with increasing temperature in the microwave region for all materials studied.
- (4) At high modifier concentrations, the shift in the frequency range of the loss maxima, as well as the increase in their intensity, is less than at low concentrations. This indicates an improvement in the temperature stability of the complex dielectric or magnetic permeability of the material with increasing modifier concentration.
- (5) By varying the external temperature as well as the concentration of Ho in ceramic solid solutions of BiFeO_3 , it is possible to shift the frequency at which the maximum microwave absorption is observed.
- (6) The microstructural features at high Ho content ($x = 0.30\text{--}0.50$) have no visible effect on the absorption properties of the objects studied

It is advisable to use the results obtained in the development of new functional materials based on BiFeO_3 , as well as devices with thermally controlled frequency.

Author Contributions: Conceptualization, K.A., A.P. and L.R.; Validation, A.L. and Y.R.; Formal analysis, A.L., Y.R. and P.A.; Investigation, K.A., P.A., A.P., L.S., I.A. and A.N.; Data curation, I.A., A.L., L.R. and Y.R.; Writing—original draft preparation, K.A., P.A. and A.P.; Writing—review and editing, L.R., A.L. and Y.R.; Visualization, I.A. and E.G.; Resources: E.G. All authors have read and agreed to the published version of the manuscript.

Funding: This research was funded by Russian Science Foundation (RSF)—research project No. 23-22-00229. <https://rscf.ru/project/23-22-00229/>, accessed on 17 January 2023.

Data Availability Statement: The original contributions presented in the study are included in the article, further inquiries can be directed to the corresponding authors.

Acknowledgments: Work was performed using the equipment of the Center for Collective Use “Electromagnetic, Electromechanical and Thermal Properties of Solids”, Research Institute of Physics, Southern Federal University.

Conflicts of Interest: The authors declare no conflict of interest.

References

1. Smolenski, G.A.; Chupis, I.E. Ferroelectromagnets. *Sov. Phys. Usp.* **1982**, *25*, 475–493. [[CrossRef](#)]
2. Sen, A.; Hasan, M.K.; Islam, Z.; Hassan, M.R.A.; Zaman, T.; Matin, M.A.; Gulshan, F. Influence of Ba and Mo Co-Doping on the Structural, Electrical, Magnetic and Optical Properties of BiFeO_3 Ceramics. *Mater. Res. Express* **2020**, *7*, 016312. [[CrossRef](#)]
3. Rani, S.; Sanghi, S.; Agarwal, A.; Kumar, R.; Singh, O. Crystal Structure, Magnetic and Dielectric Properties of Er-Doped BiFeO_3 Ceramics. *Appl. Phys. A Mater. Sci. Process.* **2022**, *128*, 1–17. [[CrossRef](#)]

4. Zhang, H.; Liu, H.; Zhu, M.; Wu, H.; Yuan, M.; Liu, X.; Huang, Z. Selective Microwave Absorption of SiC–Si₃N₄ Porous Ceramics Prepared by Sacrificial Template Method. *Ceram. Int.* **2023**, *49*, 27604–27613. [[CrossRef](#)]
5. Kumar, S.N.; Naidu, K.C.B.; Banerjee, P.; Manjunatha, H.; Ratnamala, A.; Janardan, S. Advanced Ceramics for Microwave Absorber Applications. In *Frontiers in Ceramic Science*; Bentham Science Publishers: Sharjah, United Arab Emirates, 2020.
6. Wen, F.; Wang, N.; Zhang, F. Enhanced Microwave Absorption Properties in BiFeO₃ Ceramics Prepared by High-Pressure Synthesis. *Solid State Commun.* **2010**, *150*, 1888–1891. [[CrossRef](#)]
7. Carvalho, T.T.; Tavares, P.B. Synthesis and Thermodynamic Stability of Multiferroic BiFeO₃. *Mater. Lett.* **2008**, *62*, 3984–3986. [[CrossRef](#)]
8. Hou, Z.-L.; Zhou, H.-F.; Kong, L.-B.; Jin, H.-B.; Qi, X.; Cao, M.-S. Enhanced Ferromagnetism and Microwave Absorption Properties of BiFeO₃ Nanocrystals with Ho Substitution. *Mater. Lett. J.* **2012**, *84*, 110–113. [[CrossRef](#)]
9. Li, Y.; Xiaoyong, F.; Cao, M. Thermal Frequency Shift and Tunable Microwave Absorption in BiFeO₃ Family. *Sci. Rep.* **2016**, *6*, 24837. [[CrossRef](#)] [[PubMed](#)]
10. Tian, C.; Yao, Q.; Tong, Z.; Zhou, H.; Rao, G.; Deng, J.; Wang, Z.; Wang, J. Effects of Sm-Doping on Microstructure, Magnetic and Microwave Absorption Properties of BiFeO₃. *J. Rare Earths* **2020**, *39*, 835–843. [[CrossRef](#)]
11. Abubakarov, A.G.; Reyzenkind, J.A.; Hasbulatov, S.V.; Reznichenko, L.A.; Shilkina, L.A.; Verbenko, I.A.; Kleschenkov, A.B.; Pavlenko, A.V. Microwave absorption in BiFeO₃/REE (REE = Dy, Ho, Tb) solid solutions with morphotropic phase boundaries. In Proceedings of the 2016 International Conference on “Physics, Mechanics of New Materials and Their Applications”, Surabaya, Indonesia, 19–22 July 2016; Parinov, I.A., Chang, S.-H., Jani, M.A., Eds.; Nova Science Publishers, Inc.: New York, NY, USA, 2016; pp. 267–270.
12. Okadzaki, K. *Tekhnologiya Keramicheskikh Dielektrikov*; Energiya: Moscow, Russia, 1976; p. 336. (In Russian)
13. Khasbulatov, S.; Cherpakov, A.; Parinov, I.; Andryushin, K.; Shilkina, L.; Aleshin, V.; Andryushina, I.; Mardaliev, B.; Gordienko, D.; Verbenko, I.; et al. Destruction Phenomena in Ferroactive Materials. *J. Adv. Dielectr.* **2020**, *10*, 1–9. [[CrossRef](#)]
14. Guinier, A.; *Theorie et Technique de la Radiocristallographie*, 2nd ed.; Dunod: Malakoff, Paris, 1956.
15. Cojocar, V.; Markell, D.; Capwell, J.; Weller, T.; Dunleavy, L. Enhancing the Simulation Accuracy of RF Designs with Consistent Characterization and Modeling Techniques. In Proceedings of the 59th ARFTG Conference Digest, Spring 2002, Seattle, WA, USA, 7 June 2002; IEEE: Piscataway, NJ, USA, 2002; pp. 147–153.
16. Capwell, J.; Weller, T.; Markell, D.; Dunleavy, L. Automation and real-time verification of passive component S-parameter measurements using loss factor calculations. *Microw. J.* **2004**, *47*, 82–90.
17. Wang, Z.; Zhao, G.L. Electromagnetic Wave Absorption of Multi-Walled Carbon Nanotube-Epoxy Composites in the R Band. *J. Mater. Chem. C* **2014**, *2*, 9406–9411. [[CrossRef](#)]
18. Astafev, P.; Pavelko, A.; Andryushin, K.; Lerer, A.; Reizenkind, J.; Reznichenko, L. Microwave Electrodynamic Study on Antiferroelectric Materials in a Wide Temperature Range. *Materials* **2022**, *15*, 8834. [[CrossRef](#)] [[PubMed](#)]
19. Bokij, G.B. *Vvedeniye V Kristallokhimiyu*; Izdatel'stvo Moskovskogo Universiteta: Moscow, Russia, 1954. (In Russian)
20. Urusov, V.S. *Teoriya Izomorfnoy Smesimosti*; Nauka Moscow, USSR: Moscow, Russia, 1977; p. 251. (In Russian)
21. Fesenko, E.G. *Semejstvo Perovskita i Segnetoehlektrichestvo*; Atomizdat: Moscow, Russia, 1972; p. 248. (In Russian)
22. Hornstra, J. The Role of Grain Boundary Motion in the Last Stage of Sintering. *Physica* **1961**, *27*, 342–350. [[CrossRef](#)]
23. Available online: https://materials.springer.com/isp/phase-diagram/docs/c_1101985 (accessed on 24 October 2023).

Disclaimer/Publisher's Note: The statements, opinions and data contained in all publications are solely those of the individual author(s) and contributor(s) and not of MDPI and/or the editor(s). MDPI and/or the editor(s) disclaim responsibility for any injury to people or property resulting from any ideas, methods, instructions or products referred to in the content.